The impact of spatiotemporal structure of rainfall on flood frequency over a small urban watershed: an approach coupling stochastic storm transposition and hydrologic modeling

Zhengzheng Zhou[1], James A. Smith[2], Mary Lynn Baeck[2], Daniel B. Wright[3], Brianne K. Smith[4], Shuguang Liu[1]

[1]Department of Hydraulic Engineering, Tongji University, Shanghai, China.
[2]Department of Civil and Environmental Engineering, Princeton University, USA.
[3]Department of Civil and Environmental Engineering, University of Wisconsin-Madison, USA.
[4]Department of Earth and Environmental Sciences, City University of New York-Brooklyn College, USA.

Corresponding to: Zhengzheng Zhou (zhouzz@tongji.edu.cn); Shuguang Liu (liusgliu@tongji.edu.cn)

Abstract. The role of rainfall space-time structure, as well as its complex interactions with land surface properties, in flood response remains an open research issue. This study contributes to this understanding, specifically in small (<15 km^2) urban watersheds. Using a flood frequency analysis framework that combines stochastic storm transposition-based (SST) rainfall scenarios with the physically-based distributed GSSHA model, we examine the role of rainfall spatial and temporal variability in flood frequency across drainage scales in the highly-urbanized Dead Run watershed (14.3 km^2), Maryland, USA. The results show the complexities of flood response within several subwatersheds for both short (<50 years) and long (>100 years) rainfall return periods. The impact of impervious area on flood response decreases with increasing rainfall return period. For extreme storms, the maximum discharge is closely linked to the spatial structure of rainfall, especially storm core spatial coverage. The spatial heterogeneity of rainfall increases flood peak magnitudes by 50% on average at the watershed outlet and its subwatersheds for both small and large return periods. The framework of SST-GSSHA-coupled frequency analysis also highlights that spatially-distributed rainfall scenarios are needed in quick-response flood frequency even for relatively small basin scales.

1. Introduction

Rainfall spatiotemporal structure plays an important role in flood generation in urban watersheds (Saghafian *et al.*, 1995; Smith *et al.*, 2005b; Emmanuel *et al.*, 2012; Nikolopoulos *et al.*, 2014). Spatial heterogeneities in land use and land cover complicate the translation of rainfall spatiotemporal distribution into flood responses (Galster *et al.*, 2006; Morin *et al.*, 2006; Ntelekos *et al.*, 2008; Ogden *et al.*, 2011; Yin *et al.*, 2016; ten Veldhuis *et al.*, 2018), especially for small catchments (Faurès *et al.*, 1995; Smith *et al.*, 2005a; Zhou *et al.*, 2017; Zhou *et al.*, 2019; Yang *et al.*, 2020). The influence of rainfall spatial-temporal structure on flood frequency analysis in urban areas remains an open research issue.

Previous studies have demonstrated the sensitivity of hydrological response to rainfall variability in both space and time (Smith *et al.*, 2012; Ochoa-Rodriguez *et al.*, 2015; Rafieeinasab *et al.*, 2015). Following the advent of rainfall measurement using weather radar (Fulton *et al.*, 1998; Krajewski and Smith, 2002), many studies have highlighted the use of high-resolution rainfall data in assessing rainfall variability over various range of spatial and temporal scales (Berne *et al.*, 2004; Gebremichael and Krajewski, 2004; Moreau *et al.*, 2009; Emmanuel *et al.*, 2012) and how their use could improve runoff estimation (Morin *et al.*, 2006; Smith *et al.*, 2007; Schellart *et al.*, 2012; Wright *et al.*, 2014b; Rafieeinasab *et al.*, 2015; Gourley *et al.*, 2017).

There are conflicting findings on the relative importance of rainfall temporal and spatial characteristics. Paschalis *et al.* (2014), Ochoa-Rodriguez *et al.* (2015) and Yang *et al.* (2016) found that "coarsening" temporal resolution has a stronger impact than coarsening spatial resolution. Adams *et al.* (2012) found the space-time averaging effects of routing through the catchment noticeably remove the impact of spatially variable rainfall at a 150-km^2 catchment scale. Bruni *et al.* (2015), in contrast, found a higher sensitivity of modeled flow peaks to spatial resolution rather than the temporal resolution. Peleg *et al.* (2017) showed an increasing contribution of the spatial variability of rainfall to the variability of flow discharge with longer return periods. Cristiano *et al.* (2018); Cristiano *et al.* (2019) found the spatial aggregation of rainfall data can have a strong effect on hydrological responses. Zhu *et al.* (2018) examined the influence of rainfall variability on flood frequency analysis and addressed the impact of antecedent moisture in flood generation for various basin scales.

Stochastic Storm Transposition (SST) was developed as a physically-based stochastic rainfall generator for rainfall frequency analysis. Previous studies show that SST with relatively short rainfall records (10 or more years) of high-resolution radar rainfall fields can produce reasonable rainfall scenarios with realistic spatial-temporal structure, which cannot be provided by conventional design storm methods. In the conventional approach, the idealized assumtions include idealized rainfall temporal structure, uniformed spatial distribution and 1:1 rainfall-flood return periods equivalence (see (Wright *et al.*, 2013; Wright *et al.*, 2017; Zhou *et al.*, 2019), and references therein). These assumtions ignore the interaction between spatiotemporal structure of rainfall and flood responses, which increases the uncertainty of frequency estimations. Coupled with hydrological models, the SST-based framework can be used for multiscale rainfall frequency analysis and flood frequency analysis that accounts for rainfall variability and surface characteristics (Wright *et al.*, 2014a; Perez *et al.*, 2019; Yu *et al.*, 2019; Wright *et al.*, 2020).

Previous studies have demonstrated the relationship between rainfall and flood are scale-dependent, varying with rainfall patterns, basin characteristics, and runoff generation processes. However, there is still no clear answer on the relative importance of temporal and spatial features of rainfall on flood responses (Cristiano *et al.*, 2017). Moreover, studies focusing on small (<15 km^2) urbanized basins are relatively few (Peleg *et al.*, 2017) and the issues remain poorly understood.

This study contributes to the understanding of the interaction between rainfall variability and flood response over small-scale urbanized watersheds (<15 km^2) for a short-duration rainfall and quick hydrologic response setting. We build on the SST-based rainfall study of Zhou *et al.* (2019) using the physically-based hydrological model implementation introduced by Smith *et al.* (2015) for the Dead Run watershed outside of Baltimore, Maryland, USA. The framework of SST-based rainfall frequency analysis coupled with a hydrological model provides an effective approach for detailed flood frequency study (Wright *et al.*, 2014a; Yu *et al.*, 2019). Under the framework, we characterize the spatial and temporal features of rainfall events under different return periods and examine their roles in determining flood frequency in small urban watersheds. The following questions will be addressed: (1) How does flood frequency in small urban watersheds vary with diverse space-time rainfall structure and rainfall magnitude? (2) What are the dominant space-time feature of rainfall that control flood peak distribution in small urban watersheds? By answering the above questions, the study can improve the understanding of interactions between rainfall and flood process in small urbanized area. In addition, some idealized assumption used in the convetional rainfall-flood frequencny analysis will be questioned.

The paper is organized as follows: in Section 2, we introduce the study region and describe the SST-based methodology, GSSHA model, and the metrics used to characterize rainfall and flood response. In Section 3, we present model validation and analyses of flood frequency distributions and rainfall-flood relationships. A summary and conclusions are presented in Section 4.

2. Data and method

2.1 Study region and data

The study focuses on the highly-urbanized 14.3 km^2 Dead Run (DR) watershed located west of Baltimore, Maryland, USA (Fig. 1). DR is a tributary to the Gwynns Falls watershed, which is the principal study catchment of the Baltimore Ecosystem Study (BES; Pickett and Cadenasso (2006). The basin has an impervious fraction of approximately 52.3% (Table 1). The watershed has a dense network of six stream gauges with drainage areas ranging from 1.2 to 14.3 km^2 (Fig. 1; Table 1). The subwatersheds are developed after the implementation of the Maryland Stormwater Management Act of 1982 (Maryland, 1982) with many detention infrastructures such as small local ponds. The wealth of data for Dead Run provides exceptional resources to examine rainfall and hydrologic response (Beighley and Moglen, 2002; Nelson *et al.*, 2006; Meierdiercks *et al.*, 2010; Smith *et al.*, 2015). For example, Meierdiercks *et al.* (2010) analyzed the impact of storm drains and detention basins on a single storm event in DR, while Ogden *et al.* (2011) used the Gridded Surface Subsurface Hydrologic Analysis (GSSHA) model to analyze the effects of storm drains, impervious area, and drainage density on hydrologic response. Smith *et al.* (2015) created a DR model using GSSHA to examine the effects of storage and runoff

generation processes through analyses of a large number of storm events.

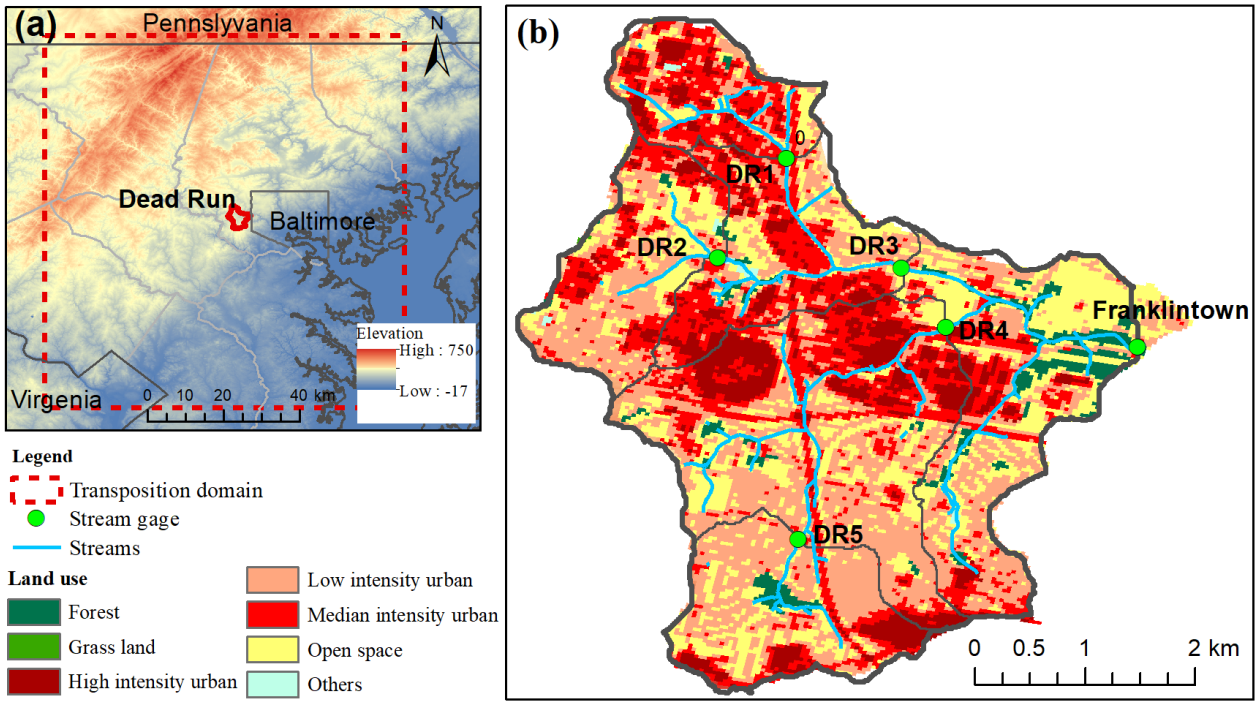

Figure 1. Overview of Dead Run study region including (a) location of DR, elevation, and transposition domain of SST; (b) land use land cover and stream gages. The red outline and grey outline in (a) indicates the boundary of DR watershed and Baltimore City, respectively.

High resolution (15-min temporal resolution, 1-km^2 spatial resolution) 34radar rainfall fields for the 2000-2015 period were derived from volume scan reflectivity fields from the Sterling, Virginia WSR-88D (Weather Surveillance Radar-1988 Doppler) radar. The two-dimentional radar rainfall fields are then developed from the reflectivity fields using the Hydro-NEXRAD algorithms (Krajewski *et al.*, 2011) which have been used in rainfall and hydrological studies (Smith *et al.*, 2007; Lin *et al.*, 2010; Smith *et al.*, 2013; Wright *et al.*, 2014b; Zhou *et al.*, 2017)he Hydro-NEXRAD algorithms includes quality control algorithms, *Z-R* conversion of reflectivity to rainfall rate, time integration, and spatial mapping algorithms (Seo *et al.*, 2011). To improve the rainfall estimates, a multiplicative mean-field bias correction (Smith and Krajewski, 1991; Wright *et al.*, 2012) is applied on a daily basis using a network of 54 rain gauges in and around the Baltimore County. The bias computation takes the form $B_i = \frac{\sum_{S_i} G_{ij}}{\sum_{S_i} R_{ij}}$. Where G_{ij} is the rainfall accumulation for gage j on day i, R_{ij} is the daily rainfall accumulation for the co-located radar pixel accumulation on day i, and S_i is the index of the rain gage stations for which both the rain gage and the radar report positive rainfall accumulations for day i. Each 15-min radar rainfall field from day i is then multiplied by B_i. The reader is directed to Zhou *et al.* (2019) and references therein for further details on the rainfall data and bias correction methods.

Instantaneous discharge data with a resolution of five minutes from the U.S. Geological Survey (USGS) were used for DR-

1, DR-2, DR-5, and Franklintown. For DR-3 and DR-4, the discharge data is converted through stage discharge curves from (Lindner and Miller, 2012). Streamflow observations for the outlet station at Franklintown extend back to 1960. The subwatersheds have records beginning in 2008.

Table 1: Characteristics of Dead Run watershed (Smith *et al.*, 2015)**.**

	USGS ID	Area (km^2)	Developed Land[a] (%)	Imperviousness (%)	Dentention controlled area[b] (%)
DR1	01589317	1.32	99%	73.6	41.9
DR2	01589316	1.92	98%	55.5	18.5
DR3	01589320	4.95	98%	62.2	24.4
DR4	01589315	6.29	98%	51.5	12.2
DR5	01589312	2.05	96%	47.9	3.2
Franklintown	01589330	14.3	96%	52.3	25.1

Note:

a. Developed lands include "Developed, open space" (>20% impervious surface), "Developed, low intensity" (20%-49% impervious surface), "Developed, medium intensity" (50%-79% impervious surface), and "Developed, high intensity" (80% or more impervious surface). Data source: USGS 2012 National Land Cover Dataset (NLCD).

b. Dentention controlled areab refers to the area controlled by detention infrastructure.

2.2 GSSHA Hydrological Model

The distributed physics-based GSSHA model is used to simulate multi-scale flood response. GSSHA is a two-dimensional, distributed-parameter raster-based (i.e. square computational cell-based) hydrologic modeling system. It uses explicit finite difference and finite volume methods in two dimensions on a structured grid to simulate overland flow and in one dimension to simulate channel flow (Downer and Ogden, 2004; 2006). Previous studies of the GSSHA model show that the model with fine grid resolution can produce adequate simulations of flood response, especially when driven by high-resolution radar rainfall fields (Sharif *et al.*, 2010; Sharif *et al.*, 2013; Wright *et al.*, 2014a; Cristiano *et al.*, 2019).

In this study, we use the Dead Run model created by Smith *et al.* (2015). A brief description of the model is provided here; see Smith *et al.* (2015) for more details. The delineation of the watershed and channel network was based on a 30-m USGS digital elevation model (Gesch *et al.*, 2002). Channel flow overland flow was set with different Manning's roughness coefficients. Additional stream channels were added based on the Baltimore County hydrography Geographic Information Systems (GIS) map. Stream cross sections were extracted from a 1-m resolution topography data set for Dead Run developed from lidar. Storm sewers in DR-2 and DR-5 were added using the Baltimore County Stormwater Management

GIS map and digitized storm sewer maps. The semicircle's diameter was set to the pipe diameter. Detention basins were represented within the channel with cross sections extracted from the 1-m lidar topographic data.3

Several aspects of the model were modified from those used in Smith *et al.* (2015), primarily to improve computational speed. Infiltration is calculated using Richards' equation (RE) in Smith *et al.* (2015), while this study uses the three-layer Green-Ampt (GA) scheme. A uniform Manning's roughness coefficient of 0.01 is set for all the stream channels for model simplification. Initial soil moisture is approximated to be one third of field capacity for each storm event.

2.3 SST procedure

The rainfall scenarios in this study are developed using RainyDay, an open-source SST software package (Wright *et al.*, 2017). The steps used are briefly summarized here; the reader is directed to Zhou *et al.* (2019) and references therein for further details.

The first step is to identify a geospatial "transposition domain" that contains the watershed of interest. In this study, we use a square 7,000 km^2 transposition domain centered on the DR watershed. (Zhou *et al.*, 2019) presented a detailed examination of heterogeneity in extreme rainfall over the transposition domain using a variety of metrics, including storm counts, mean storm depths and intensities, convective activity indicated by lightning observations, and analysis of spatial and temporal rainfall structure.

The second step is to identify the largest m storms within the domain at the t-hr time scale. This collection of storms is referred to as a storm catalog. The storms are selected with respect to the size, shape and orientation of the DR watershed. We henceforth refer to these as "DR-shaped storms." The m DR-shaped storms are selected from an n-year rainfall record, such that an average of $\lambda=m/n$ storms per record year are included in the storm catalog. In this study, we chose m = 200 storms over the 16-year radar record.

The third step is to randomly sample a subset of k storms from the storm catalog, where k refers to a stochastic number of storms per year. The k is assumed to follow a Poisson-distributed number of storm occurrences with rate parameter $\lambda=m/n$ storms per year. All rainfall fields associated with a storm are transposed by an east-west distance Δx and a north-south distance Δy, where Δx and Δy are drawn from distributions $D_X(x)$ and $D_Y(y)$ which are bounded by the limits of the transposition domain. Based on the spatial heterogeneity analysis of extreme rainfall in the domain, distributions $D_X(x)$ and $D_Y(y)$ can be set as uniform or non-uniform. In Zhou *et al.* (2019) and this study, since the assumption of regional homogeneity cannot be relaxed, we used the non-uniform distribution. A two-dimensional probability density function (PDF) of spatial storm occurrence (Wright *et al.*, 2017) is used as the basis for non-uniform spatial transposition (Fig. A1 in Appendix A). This step can be understood as generating a "synthetic year" of extreme rainfall events over the domain

based on resampling and transposing observations. For each of the k transposed storms, compute the t-hr basin-average rainfall depth over the watershed. Among the k rainfall depths, the maximum depth is retained as a synthetic t-hr annual rainfall maximum for the watershed, while the transposed rainfall fields are saved for use as inputs to a GSSHA model simulation.

The fourth step repeats Step 3 S times to recreate multiple years of synthetic t-hour "annual" rainfall maxima and associated transposed rainfall fields for the watershed. In this study, these steps are repeated S =300 times and the ordered "annual" maxima are used to generate rainfall return period estimates up to 200 years. 300 such realizations of 200-yr series are generated, and the median value of 300 realizations are used to generate estimates for return periods up to 200 years.

2.4 Characteristics of rainfall and hydrologic response

2.4.1 Spatio-temporal characteristics of rainfall

Rainfall statistics were computed for each event, based on radar rainfall data at 15-min, 1-km^2 resolution, to characterize the spatial and temporal variability of rainfall (following Smith *et al.* (2002); Smith *et al.* (2005b); see also Zoccatelli *et al.* (2011) and Emmanuel *et al.* (2015)). For basin scale of A, the basin-average rainfall rate (mm/h) at time t during the storm is given by:

$$\mathrm{M(t)} = \int_A R(t,x)dx \tag{1}$$

where $R(t,x)$ is the rain rate at radar grid x at time t, and T is the time period of rainfall event. Peak basin-average rainfall rate (mm/h) is denoted:

$$\mathrm{M}_{max} = \max\{\mathrm{M(t)}; t \in [0,T]\} \tag{2}$$

and storm total rainfall depth (mm) is:

$$\mathrm{R}_{sum} = \sum_0^T M(t) \tag{3}$$

To characterize the spatial properties of rainfall, several dimensionless quantities are computed. Fractional coverage of storm core at t is given by:

$$\mathrm{Z(t)} = \frac{1}{A}\int_A I_{(R(t,x))}dx \tag{4}$$

where $I_{(R(t,x))}$ is the indicator function and equals 1 when $R(t,x) > 25\ mm/h$ or 0 otherwise.

Rainfall location is given by:

$$\mathrm{L(t)} = \int_A \omega(t,x)d(x)dx \quad (5)$$

where $\omega(t,x) = \frac{R(t,x)}{\int_A R(t,x)dx}$, $d(x)$ is the linear distance from point x to the outlet. The rainfall-weighted flow distance is:

$$\mathrm{RWD(t)} = \int_A \omega(t,x)d_f(x)dx \quad (6)$$

where distance function $d_f(x)$ is the flow distance between point x and the outlet. It is calculated as the sum of the overland flow distance from *x* to the nearest channel and the distance along the channel to the basin outlet. The flow distance $d_f(x)$ is normalized by the maximum flow distance, ranging from 0 to 1. RWD with values close to 0 indicates that rainfall is distributed near the basin outlet; with values close to 1 indicates rainfall concentrated at the far periphery of the basin. For a uniformly distributed rainfall, the mean RWD is:

$$\overline{\mathrm{RWD}} = \int_A d_f(x)dx \quad (7)$$

The dispersion of RWD:

$$\mathrm{S(t)} = \frac{1}{\bar{s}}\int_A \omega(t,x)[d_f(x) - \bar{d}]^2dx \quad (8)$$

where $\bar{s} = \int_A [d_f(x) - \bar{d}]^2dx$, S is a spatial indicator with values < 1 indicates that rainfall is a unimodal distribution,that is, spatially one peak over the watershed; S with values >1 indicates that rainfall is a multimodal distribution.

The Eqs.1-3 are typical rainfall characteristics used in conventional rainfall-flood analysis since they reflect the general information of rainfall. Since the basin-averaged index will ignore the potential spatial heterogeneity over the watershed, Eqs. 4-8 describe the spatial distribution of rainfall within the area.

2.4.2 Spatiotemporal characteristics of hydrologic response

Flood peak (Q_{peak}, mm^3/s), total runoff (Q_{sum}, mm), and lag time (T_{lag}, min) are defined as:

$$\mathrm{Q}_{peak} = \max\{ Q(t); t \in T_d\} \quad (9)$$

$$\mathrm{Q}_{sum} = \sum_0^{T_d} Q(t) \quad (10)$$

$$T_{lag} = T_{Fpeak} - T_{Rpeak} \quad (11)$$

Respectively, where $Q(t)$ is the flow discharge at time *t*; T_d is the duration of hydrological response, which is from the start of rainfall event to the time when $f(t)<0.05*Q_{peak}$.

3. Results and Discussion

3.1 Model validation

We validated the Dead Run GSSHA model through analyses of the 21 largest warm season (April-September) flood events with peak discharges ranging from 70.3 to 253 m^3/s in the 2008-2012 period. The simulated discharge was compared to USGS streamflow observations for all six gaging stations. We assessed peak discharge, peak time and Nash-Sutcliffe Efficiency (NSE) (Nash and Sutcliffe, 1970) to examine the performance of the model.

Peak discharge difference is calculated as the difference between the modeled peak and measured peak as a percentage of the measured peak (Fig. 2a). The peak discharge is underestimated at DR2, DR4, DR5 and Franklintown. The median peak discharge difference at the downstream Franklintown gage was -14%. For the subwatersheds, the modeled peak at DR2 matches observation best with a median difference of -7.8%. This represents relatively good performance in reproducing peak discharges for such a large collection of flood events with various peak discharges ranging from 70 m^3/s to 253 m^3/s. The peaks at DR1 are overestimated substantially by 57% on average. The issue at DR1 was shown before in (Smith *et al.*, 2015) who speculate that the watershed contains a large land area which is not represented fully on county storm sewer maps.

The peak time difference is calculated as the time difference between the simulated peak time and measured peak time (Fig. 2b). The median difference ranges from -15 min to +10 min, which is within the temporal resolution of the data (15 min for rainfall; 5 min for streamflow). It should be noted that there are several large peak time differences occurred within the 21 storm events. These are due to the storms that produce multiple discharge peaks. The measured discharge may have the first peak as the largest while the modeled discharge has the next peak as the largest which is hundreds of minutes later. Nontheless, the figure shows that the timing of the peak fow is well captured by the model.

The median Nash-Sutcliffe Efficiency (NSE) for the 21 events at Franklintwon is 0.77 (Fig. 2c). The best NSE at Franklintown is 0.97 indicating that the match between model and measured data was nearly exact. For the subwatersheds, the best median NSE is at DR-4 with a value of 0.74, while the least median NSE is at DR-1 with a value of 0.21. The results show that the main tendency of flood response is captured by the model.

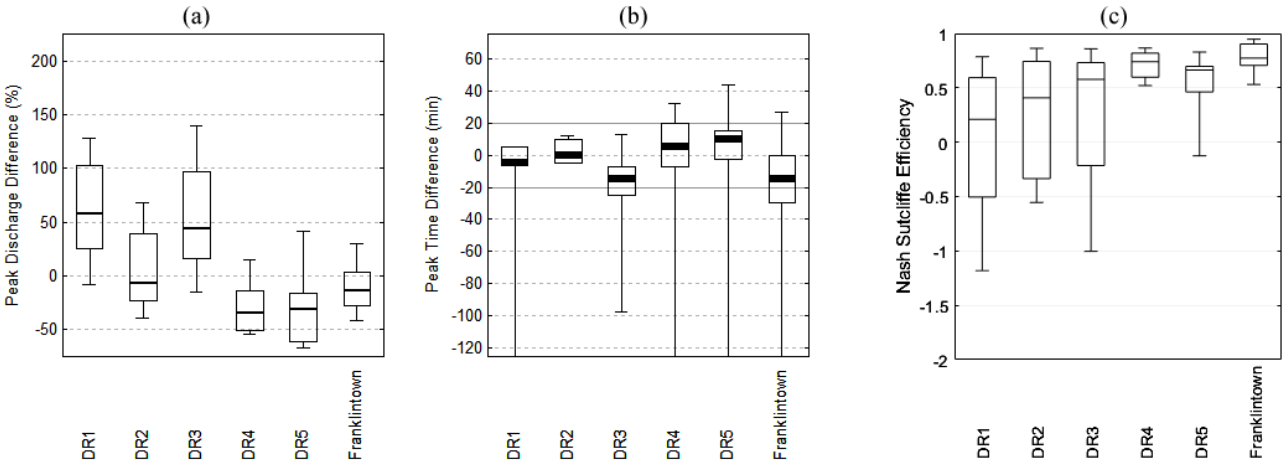

Figure 2. Comparison of (a) flood peak discharges, (b) response times and (c) NSE for 21 historical rainfall events.

The hydrograph of the 14 August 2011 storm event is shown as a representative of flood simulation. The peak discharge difference is -12% at Franklintown with a NSE of 0.93. Modeled hydrographs matches the measured data well at the outlet of watershed. For the subwatersheds, the peak discharge difference ranges from -38% at DR4 to 12% at DR-1. The shape and timing of the modeled response is similar to the measured hydrograph. But the peak discharge is underestimated by more than 30% at DR-4.

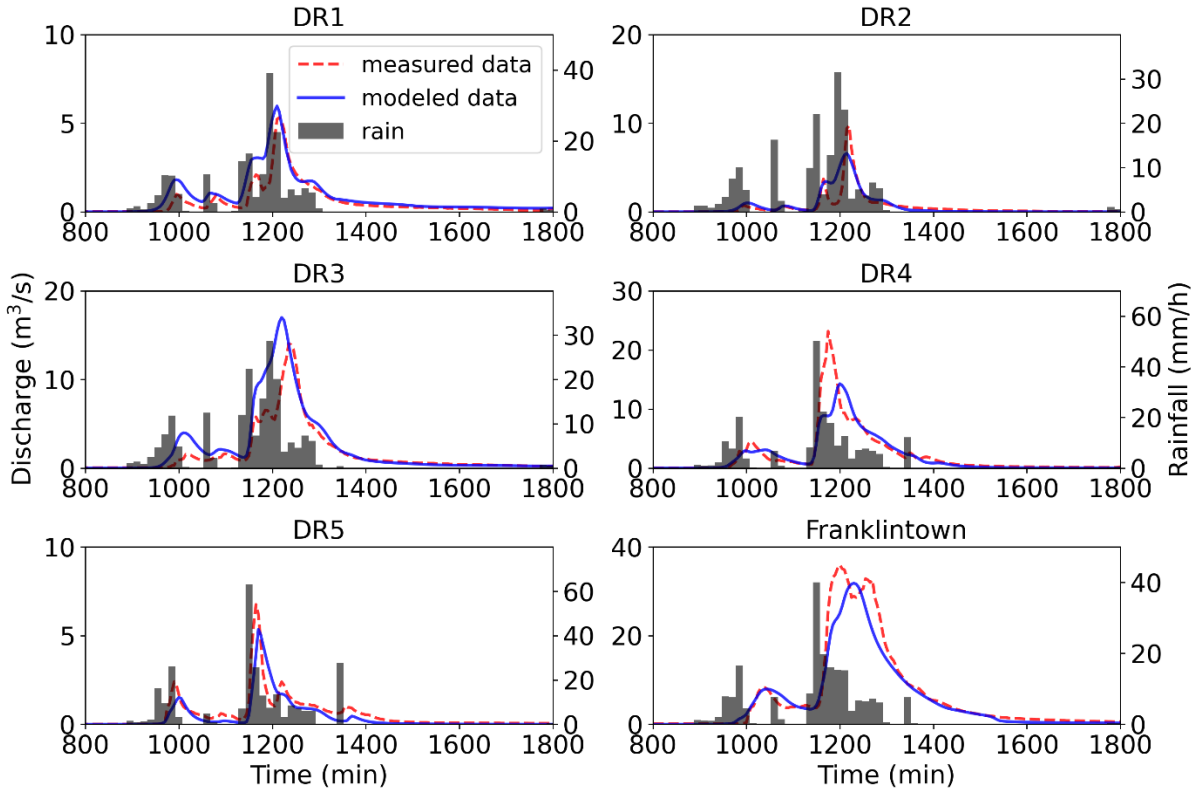

Figure 3. Hydrographs and rainfall for the the 14 August 2011 storm event. Time refers to minutes from the start of the model simulation.

237 It should be noted that the error in simulated response may be attributable to measurement errors tied to stage-discharge
238 curves and to conversions of radar reflectivity to rainfall rate, as well as to the features that were simplified within the
239 model, such as initial soil moisture and some aspects of the storm drain network (Smith *et al.*, 2015). For example, it has
240 been documented that the average error of discharge between USGS direct measurements and stage-discharge curves for
241 Franklintown is 17.4% between 2008 and 2010 (Lindner and Miller, 2012) ; this error likely grows for high flow conditions.
242 Furthermore, for the rainfall data set used in this study, the median difference of the storm total rainfall between a rain gage
243 and the bias-corrected radar rainfall data for all the pixel of gages over the 21 storms is 22.6% (Smith *et al.*, 2015). It may
244 also increase the error in the measurements and modeling results.
245 Overall, the validation shows that the hydrological model can capture the main shape and timing of the measured response
246 in Dead Run. We therefore conclude that the model is suitable for the subsequent flood frequency analysis.

247 **3.2 Flood frequency distribution**

248 Under the SST framework, 3-h rainfall scenarios for 10-yr, 50-yr, 100-yr and 200-yr return periods were generated (Fig.
249 A2 in Appendix A). For each rainfall return period, 300 realizations of rainfall events are used as input to drive the
250 hydrological model. Henceforce, for each rainfall return period, 300 flood responses can be simulated for Franklintown
251 and the five DR subwatershedss.

252 **3.2.1 Flow discharge estimates**

253 The distribution of maximum discharge at the Franklintown gage for rainfall return periods ranging from 10 to 200 years
254 is illustrated in Fig. 4a. To compare the distributions of rainfall and flood peaks, the values are normalized to range from 0
255 to 1. The normalization is the ratio of values minus the minimum to the maximum minus minimum. The most striking
256 feature is that the distributions of total rainfall and flood peaks are highly variable across the four return periods. The kernel
257 density distribution of rainfall shows a peak at the position of 50^{th} quantile for four return periods. The distribution of flood
258 peak is more complex. For the 100-yr rainfall return period, the kernel density distribution of flood peaks shows a
259 multimodal trend with two small peaks around the 25^{th} and 75^{th} quantiles, which contrasts with the unimodal distribution
260 of rainfall. The following results will show that flood peak is highly related to spatial rainfall features, implying that the
261 multimodal distribution of flood peaks is associated with the spatial distribution of rainfall. The pronounced difference in
262 the distributions of total rainfall and flood peaks highlights a complex relationship between rainfall properties and flood
263 response in this relatively small urbanized watershed.
264 The flood response time is calculated as the difference between the time of maximum rainfall rate and maximum discharge

(Fig. 4b). Median values of response time are similar under all return periods, ranging from 70 to 83 minutes, which, given the temporal resolution of rainfall is 15 minutes, can be similar for all four return periods. It can be concluded that although the flood peak magnitude increases with rainfall return period, the response time is consistent for various rainfall scenarios. This implies in this small highly urbanized watershed the response time is more linked to the drainage system rather than to rainfall characteristics.

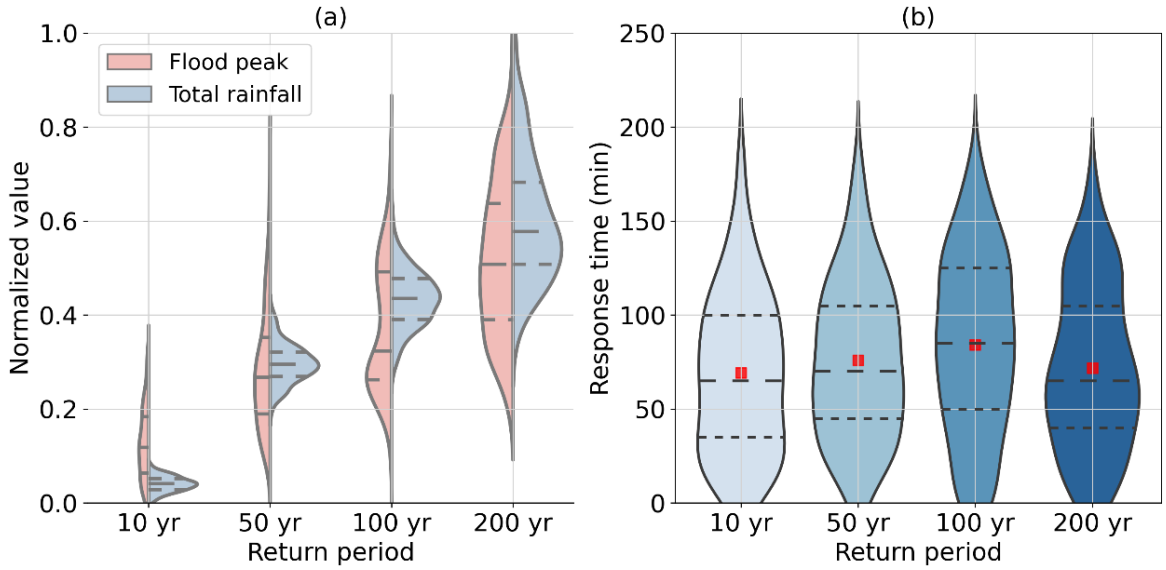

Figure 4. Violin plots of (a) normalized flood peak and normalized total rainfall; and (b) response time from 10-y to 200-y rainfall return periods. (The red dot indicates mean value. Dashed line in the middle indicates the median value. Upper and lower dashed lines indicate the 75th and 25th quantiles, respectively.) The rainfall return periods are calculated with respect to average rainfall rate over the entire DR watershed.

Figure 5 demonstrates the simulated hydrographs for the four return periods. The upper and lower spread (75th and 25th quantiles) of the hydrograph indicates the range of variability of simulated hydrographs. For the 10-yr return period, the hydrograph is relatively smooth with smaller spread. With increasing return period, the hydrograph is peakier with shorter duration of high magnitude discharge. The hydrograph for the 50-yr return period shows a transitional shape between small (10-yr) and large (100-yr and 200-yr) rainfall return periods. For the 100-yr return period, the upper spread shows a tendency toward dual peaks, which cannot be revealed from conventional design flood practices. Since in the conventional rainfall flood frequency approach, the design storm is temporally idealized as a unimodal peak process. By using theses design storm, the flood response is generally simulated as a unimodal peak process. The above results imply the uncertainty and insufficiency of flood frequency analysis in the conventional method. For the 200-yr return period, the hydrograph is peakiest with a large upper spread.

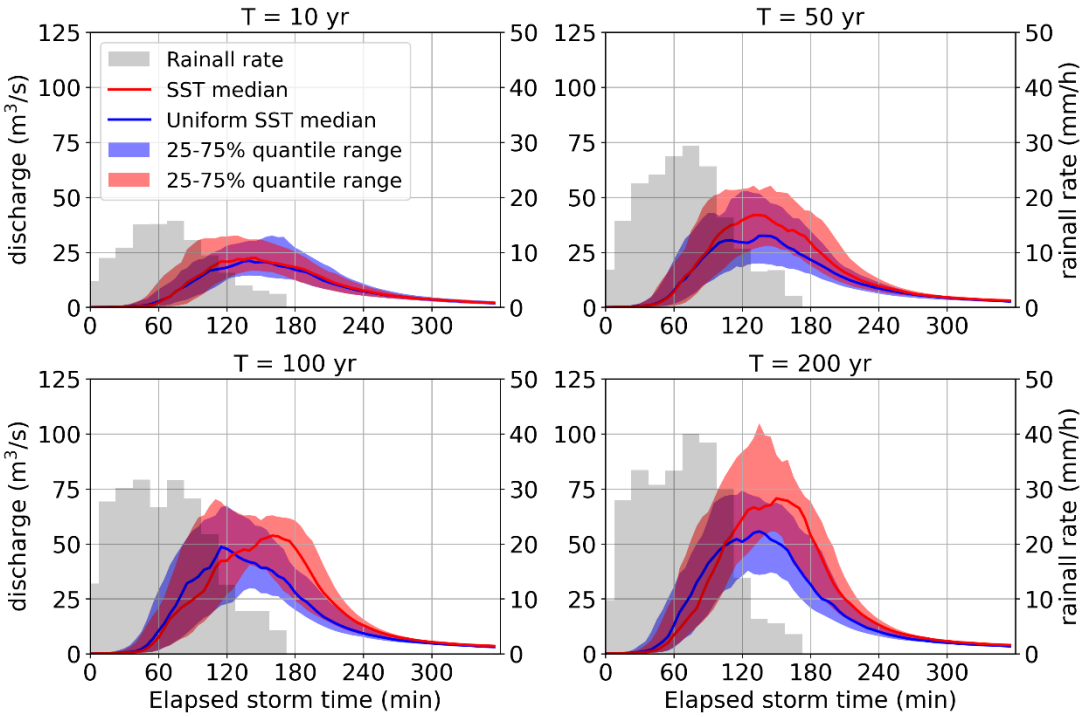

Figure 5. Time series of simulated hydrographs for Franklintown based on the 3-h design storms from 10-yr to 200-yr return periods with spatially uniform (blue) and spatially distributed (red) rainfall. The grey bar indicates the median value of basin-averaged rainfall rate.

3.2.2 Spatial distribution of flood magnitude

The distribution of flood peaks over the five subwatersheds exhibits contrasting variation with rainfall return periods ranging from 10 to 200 years (Fig. 6). Generally, basin scale plays an important role in determining the distribution of flood magnitudes. Under the 10-yr rainfall return period, DR1 and DR2, with similar basin scales of 1.32 and 1.92 km^2 respectively, have higher flood peaks and interquartile ranges than other subwatersheds. DR5 (2.05 km^2) has comparable flood magnitude with DR4 (6.3 km^2) and Franklintown (14.3 km^2), while has a larger interquartile range than the latter two. DR3 with a basin scale of 4.95 km^2, has comparable flood magnitudes with DR1 and DR2. Under the 200-yr rainfall return period, DR2 and DR3 has a slightly larger flood magnitude than DR1. DR5 has the largest interquartile range than others, though its flood peaks are smaller than other small watersheds.

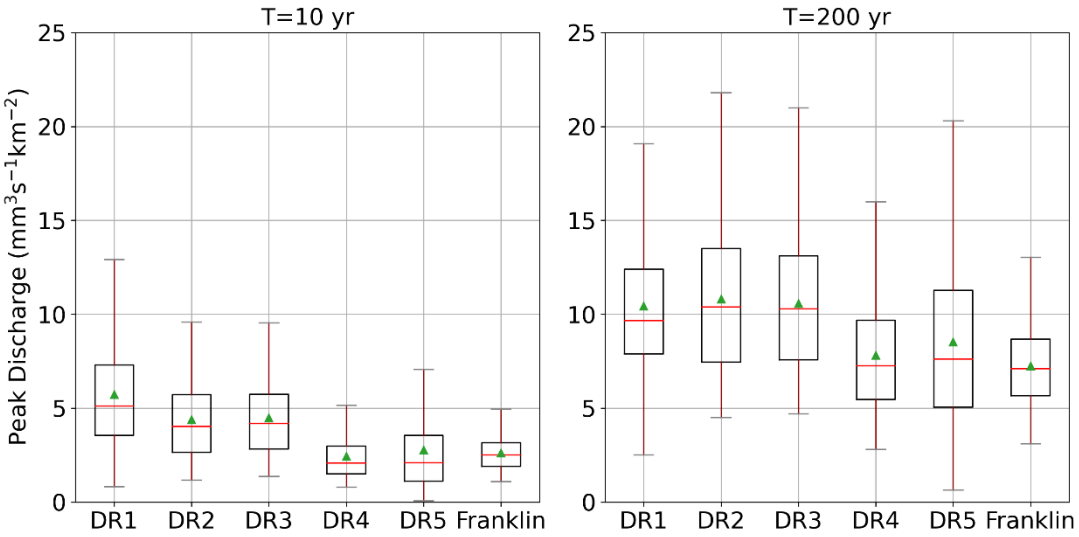

Figure 6. Boxplots of normalized flood peaks for Franklintown and five subwatersheds.

Results show that sub-basin flood distributions vary significantly with rainfall return periods. DR1 with 33% larger impervious area and more than double of dentention controlled area than DR2 (Table 1), has 26% larger median flood peak under small rainfall return period. For large return periods, DR2 has a slightly larger median peak and a larger peak and interquartile range than DR1. The contrasting peaks in DR1 and DR2 imply that flood peaks are less impacted by impervious area for extreme storms whil for small rainfall events, detention infrastreture may play a less role in the detention of flood peaks. DR5, with the smallest dentention controlled area by detention infrastructure, has the smallest flood peaks under small rainfall return period. Under large return period, however, it has the largest changes in peak discharges with comparable flood peaks with subwatersheds larger than 6 km^2. DR3 and DR4, with basin scale of 4.95 and 6.29 km^2, have contrasting flood magnitude under small and large return periods. DR3 with larger impervious area and dentention controlled area has larger flood peaks than DR4. The difference is more significant for small rainfall events with the median value of flood peak for DR3 more than double that of DR4. From these results, it implies that impervious area and dentention controlled area play a significant role in determining the peak discharges, but the impact reduces with increasing rainfall return period. The detention infrastructure impacts flood peak and its variability. It should be noted that difficulties remain in attributing specific changes in urban flood peak distributions to specific urbanization characteristics (Zhou *et al.*, 2017). The role of specific urban features in flood responses is beyond the scope of this paper.

We further examine the spatial distribution of flood magnitude over the Dead Run watershed under the 100-yr return period of flood at Franklintown (Fig. 7). The dimensionless flood index is used to compare flood peak magnitudes over the watershed (Lu *et al.*, 2017). The flood index is computed as the maximum flow discharge divided by the computed 10-yr flood ($Q_{10\text{-}y}$) at the same location, which is set as the median value of 10-yr peak discharge at the watershed outlet for each

100-yr design storm simulation. At Franklintown, the flood index and its interquartile range are largest across the watersheds, with the median value greater than 2.5. The flood index in the five sub-watersheds is relatively lower, within a median value between 1.5 and 2. DR2, as a sub-watershed of DR3, has a larger median value than DR1 and DR3. The flood indices at DR1 and DR3 have similar median values and interquartile ranges. Values in DR4 are higher than its sub-watershed, DR5, with a median value of 2. The variability of flood magnitudes, indicated by the CV, is stable among the watersheds, ranging from 0.30 to 0.39. The spatial distribution of flood magnitude points to the significant heterogeneity of flood distributions over the 14.3-km^2 watershed. For storm events that produce the same peak discharge return period at the watershed outlet, the subsequent upstream flood response can vary substantially in the Dead Run watershed.

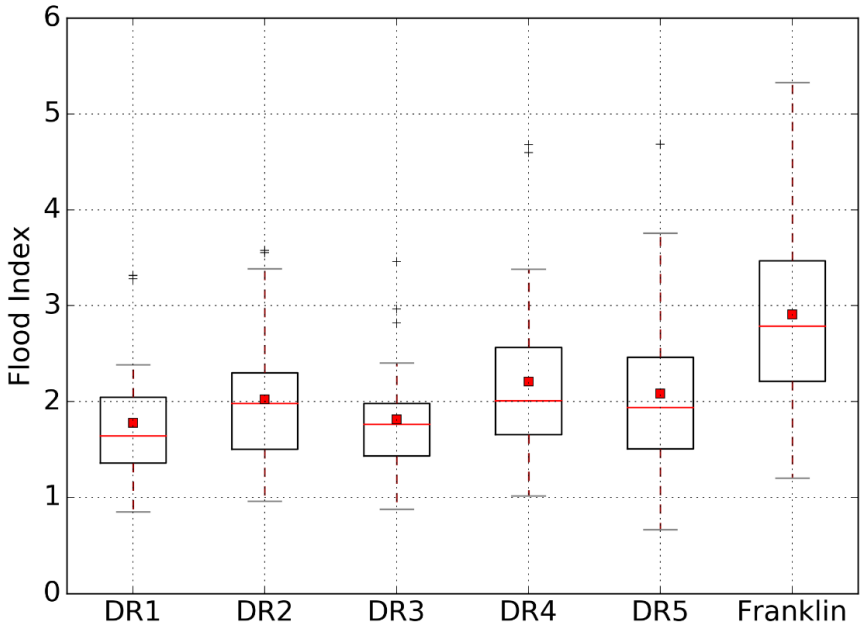

Figure 7. Boxplot of flood index across the DR subwatersheds for the 100-yr design storms.

3.3 Rainfall-Flood Relationships

3.3.1 Rainfall structure and flood response

We investigate the relationship between the spatial and temporal characteristics of rainfall and flood response for small and large rainfall return periods based on Spearman's rank correlation (Fig. A3 in Appendix A). The peak rainfall rate (M_{max}), total rainfall (R_{sum}), fractional coverage (Z), rainfall location (L), rainfall-weighted flow distance (RWD) and the dispersion of RWD (S) are used to characterize rainfall spacetime structure. For the 10-yr return period, the flood peak is slightly correlated with total rainfall, peak rainfall rate and storm core coverage with correlation coefficient of 0.16. For the 200-yr return period, in contrast, there is no significant correlation between these features with correlation coefficients of -0.09,

0.07 and -0.02, respectively, implying a complex and nonlinear relationship between extreme storms and floods in the watershed.

We used random forest regression models to examine the importance of rainfall characteristics to the flood response. Random forests (RF) is an ensemble learning method (Breiman, 2001) that aggregates results from multiple models to achieve better accuracy. RF is one of the most widely-used method for regression and classification. Moreover, it is relatively easy to train and tests. In this study, rainfall spacetime structure characteristics are used as RF model features. The flood peak is set as the model target. The relationship between rainfall structure and flood peak is then explored under the RF-based regression method. The main parameters of RF model are tuned by a grid search approach (Probst *et al.*, 2019). The prediction performance is assessed using Mean Absolute Error (*MAE*), Root Mean Square Error (*RMSE*), and explained variance regression score (*E* score) (Achen, 2017). Smaller values of *MAE* and *RMSE* indicate better model performance. *E* score ranges from 0 to 1 and a larger value indicates a better model (The training process of RF model is shown in Fig. A4 in Appendix A).

The difference in feature importance is compared between the 10-yr and 200-yr return periods (Fig. 8). For the 10-yr return period, peak rainfall rate (M_{max}) and total rainfall (R_{sum}) are the most two important features with feature importance of 0.17. For the 200-yr return period, however, the dispersion of RWD (*S*) and fractional coverage of storm core (*Z*) are more important than M_{max} and R_{sum}. The rainfall location (*L*) has the smallest importance for both return periods. The results demonstrate the different relationships between rainfall structure and flood response under small and extreme rainfall events. For extreme storms, the maximum discharge is more closely linked to the spatial structure of rainfall, which is consistent with the results in {Peleg, 2017 #313};{Zhu, 2018 #584}. Though it appears that the difference is moderate, but for a such small watershed, the tendency of the change of spatiotemperol rainfall feature importance is noteworthy.

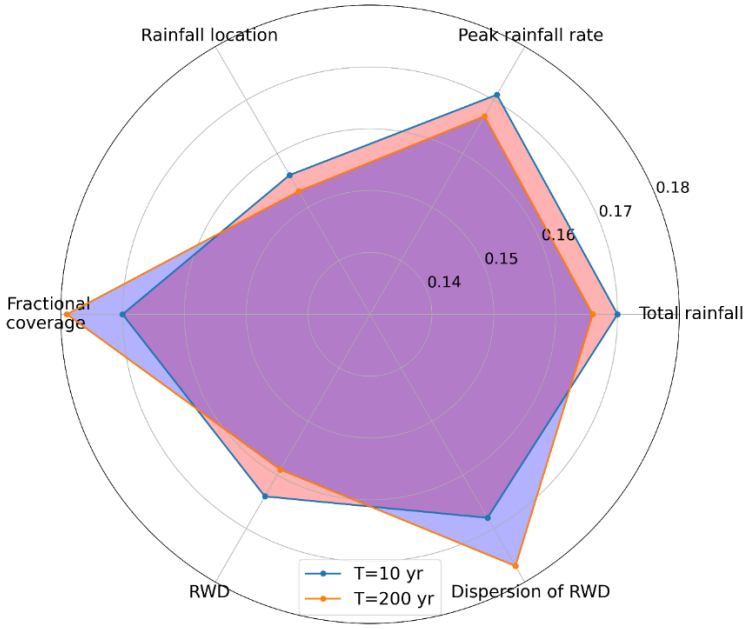

Figure 8. Feature importance analysis of RF model for space-time rainfall structure and 10-yr (red) and 200-yr (blue) flood peaks.

3.3.2 Rainfall return period vs. flood return period

In conventional design storm/flood practices, the return period of rainfall and peak discharge is often assume to be equivalent (Rahman *et al.*, 2002). Under the SST framework, we can examine this assumption (Wright *et al.*, 2014a). At the 14.3-km^2 basin scale, for each SST realization containing 100 rainfall scenarios with return period from 5 years up to 100 years, the peak discharge can be simulated and ordered. Flood frequency for return periods from 5 years up to 100 years are then estimated from the ordered peaks. We run 30 SST realizations in total. The Spearman's rank correlation of the two return periods is 0.5 (Fig. 9). The results quantitatively confirm that the assumption of a 1:1 return period equivalency between design storm and design flood cannot hold, even in a small highly-urbanized watershed where drainage network and rainfall structure play an important role in flood response. Similar results can be found between subbasins flood and DR-scale rainfall return periods (results not shown for the sake of brevity).

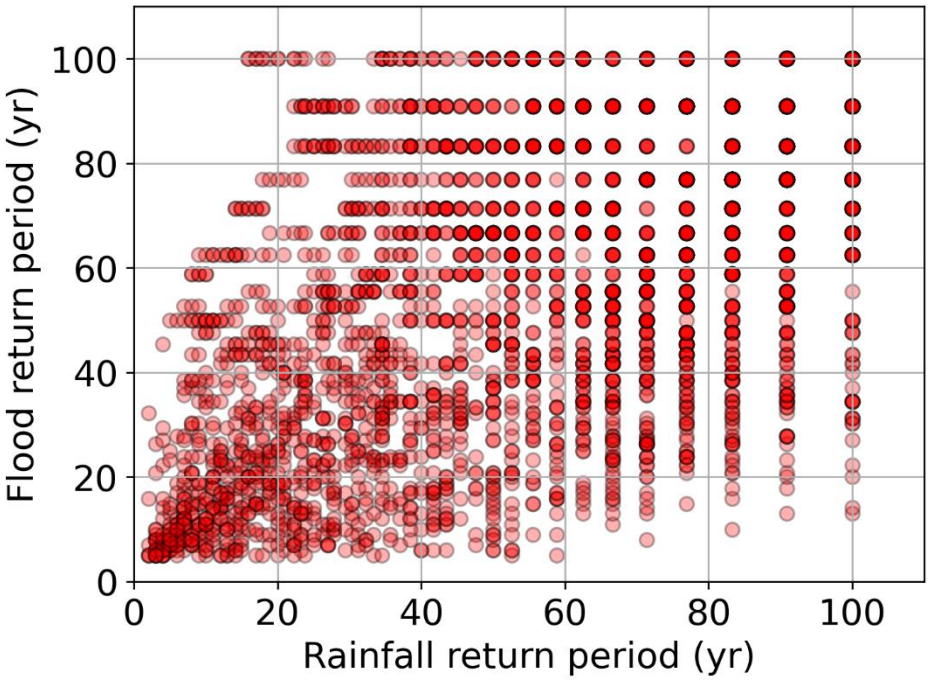

Figure 9. Scatterplot comparison return periods for rainfall and peak discharge for individual SST-based simulations.

3.3.3 Impact of rainfall spatial heterogeneity on flood responses

We also compared the simulated flood response resulting when rainfall is uniform over the watershed, rather than spatially distributed as in previous analyses (Fig. 4 and Table 2). Generally, flood peaks generated from uniform rainfall have lower peaks than for non-uniform rainfall. The difference increases with return period. Under the 10-yr return period, the shapes of the two hydrographs have similar upper and lower bounds (75% and 25% quantiles). The median flood peak using non-uniform scenarios is 22% higher than the uniform scenarios. Under the 200-yr return period, the hydrograph resulting from non-uniform rainfall is much peakier than the uniform SST scenarios with higher upper and lower bounds. The lower bound of hydrograph by non-uniform SST scenarios is close to the median hydrograph of uniform SST scenarios.

The impact of rainfall spatial heterogeneity among the five subwatersheds is different. DR1, with a basin scale of 1.32 km^2 and located in the north-west boundary of the watershed, was the least-impacted by rainfall spatial distribution for all return periods. In DR2, on the other hand, which is similar in drainage area to DR1, the flood peak increased by 46% for the 200-yr return period. For DR3 and DR4, the spatial heterogeneity of rainfall contributes more to the flood peaks in DR4 than in DR3. The most striking difference in flood peaks is in DR5 for the 50-yr return period. The difference in flood magnitude is 75%. As mentioned above, DR5 is the sub-basin with the least dentention controlled area. This finding is likely tied to the complex relationship between space-time rainfall structure and the drainage network. We can thus conclude that the

392 spatial heterogeneity of rainfall can increase flood peaks dramatically under both small and large return periods. The impact
393 increases with return period. This result shows that the assumption of spatially uniform rainfall will underestimate flood
394 frequency.

395 **Table 2. The median flood peak reductions using spatially uniform and spatially distributed rainfall.**

	T=10 yr	T=50 yr	T=100 yr	T=200 yr
DR1	14%	20%	13%	26%
DR2	19%	40%	28%	42%
DR3	24%	33%	27%	31%
DR4	32%	51%	38%	35%
DR5	15%	75%	37%	30%
Franklin	22%	36%	31%	42%

396

397 **4. Summary and conclusions**

398 This paper addresses the problem of the impacts of short-duration rainfall variability on hydrologic response in small
399 urbanized watershed. By coupling a high-resolution radar rainfall dataset and stochastic storm transposition (SST) with the
400 GSSHA distributed physics-based model (see also (Wright *et al.*, 2014a; Zhu *et al.*, 2018)), the relationships between
401 rainfall spatiotemporal structure and urban flood response is examined. The main findings are as follows:
402 1. The flood frequency distributions for subwatersheds within the highly-urbanized 14.3-km^2 Dead Run watershed
403 demonstrates complexity of flood response for both short and long rainfall return periods. For 3-h extreme storms, the large
404 variability of flood magnitude shows a pronounced role of rainfall space-time structure in flood production. This calls into
405 question the commonly-made design storm assumption of spatially uniform rainfall. The response time is less affected by
406 rainfall structure and appears to be more closely associated with the basin scale and drainage network features.
407 2. The spatial heterogeneity of flood frequency over the 14.3-km^2 watershed is striking for the 100-yr return period. The
408 intercomparison between subwatersheds show that the impact of impervious area decreases with increasing return periods.
409 For the 100-yr return period, storm events that produce the same peak discharge return period at the basin outlet can be the
410 result of very different upstream flood responses even in a small-scale watershed.
411 3. The relationship between the spacetime structure of rainfall and flood response is complex. For smaller and more frequent
412 rainfall events, flood peaks are more closely linked to the temporal features of rainfall (total rainfall and peak rainfall rate).
413 For extreme storms, the maximum discharge is closely linked to the spatial structure of rainfall (storm core coverage). This
414 finding is broadly consistent with Peleg *et al.* (2017) and Zhu *et al.* (2018), despite the very different drainage scales

considered in those studies. There is no significant correlation between rainfall peak, total rainfall and flood peaks, implying an important role of surface properties in urbanized watersheds. Similar to Wright *et al.* (2014a), this comparison calls into question the conventional design storm assumption of a 1:1 equivalency between rainfall and flood peak return periods.

4. The spatial heterogeneity of rainfall is a key driver of flood response across scales. Relative to spatially uniform rainfall, spatially distributed rainfall can increase flood peaks by 50% on average at the watershed outlet and its subwatersheds for both small and large return periods. This finding is broadly consistent with prior results at much larger scales in an agricultural setting Zhu *et al.* (2018) and suggests both spatial and temporal rainfall distributions need to be considered in flood frequency analyses, even in relatively small urban watersheds. This study also implies that the drainage network substantially alters the impact of rainfall characteristics on the runoff.

Coupling the GSSHA model and SST-based rainfall frequency analysis, this study provides an effective approach for regional flood frequency analysis for urban watersheds. Some idealized assumptions used in the conventional methods are questioned. The approach can be used to explore the dominant control on the upper tail of urban flood peaks, without many of the limiting assumptions associated with design storm methods. The study area could be extended in future work with larger basin scales and by manipulating the spatial heterogeneity of basin characteristics within GSSHA or other similar modeling systems.

Acknowledgments

This study was supported by the National Science Foundation of China (Grant 51909191).

Data availability

Radar data are archived at Princeton University and can be downloaded from the url http://arks.princeton.edu/ark:/88435/dsp01q524jr55d.

Author contributions

Main contributions from each co-authors are as follows. Zhengzheng Zhou contributed to computation and organization of the paper. James A. Smith contributed to the supervision and writing. Mary Lynn Beack is responsible for generating the radar rainfall data. Brianne K. Smith contributed to the construction of the initial hydrological model. Daniel B. Wright contributed to the writing of the paper. Shuguang Liu contributed to the supervision and writing.

Reference

Achen, C. H. (2017), What Does "Explained Variance" Explain?: Reply, *Political Analysis*, 2, 173-184.

444 doi:10.1093/pan/2.1.173
445 Adams, R., A. W. Western, and A. W. Seed (2012), An analysis of the impact of spatial variability in rainfall on runoff and
446 sediment predictions from a distributed model, *Hydrological Processes*, 26(21), 3263-3280. doi:10.1002/hyp.8435
447 Beighley, R. E., and G. E. Moglen (2002), Trend Assessment in Rainfall-Runoff Behavior in Urbanizing Watersheds,
448 *Journal of Hydrologic Engineering*, 7(1), 27-34. doi:10.1061/(ASCE)1084-0699(2002)7:1(27)
449 Berne, A., G. Delrieu, J.-D. Creutin, and C. Obled (2004), Temporal and spatial resolution of rainfall measurements
450 required for urban hydrology, *Journal of Hydrology*, 299(3), 166-179. doi:10.1016/j.jhydrol.2004.08.002
451 Breiman, L. (2001), Random Forests, *Machine Learning*, 45(1), 5-32. 10.1023/a:1010933404324
452 Bruni, G., R. Reinoso, d. G. Van, N. C., F. H. L. R. Clemens, and J. A. E. Ten Veldhuis (2015), On the sensitivity of urban
453 hydrodynamic modelling to rainfall spatial and temporal resolution, *Hydrology and Earth System Sciences*, 19(2), 691-709.
454 doi:10.5194/hess-19-691-2015, 2015
455 Cristiano, E., M. C. ten Veldhuis, and N. van de Giesen (2017), Spatial and temporal variability of rainfall and their effects
456 on hydrological response in urban areas – a review, *Hydrology and Earth System Siences*, 21(7), 3859-3878.
457 doi:10.5194/hess-21-3859-2017
458 Cristiano, E., M. C. ten Veldhuis, S. Gaitan, S. Ochoa Rodriguez, and N. van de Giesen (2018), Critical scales to explain
459 urban hydrological response: an application in Cranbrook, London, *Hydrol. Earth Syst. Sci.*, 22(4), 2425-2447.
460 doi:10.5194/hess-22-2425-2018
461 Cristiano, E., M.-c. ten Veldhuis, D. B. Wright, J. A. Smith, and N. van de Giesen (2019), The Influence of Rainfall and
462 Catchment Critical Scales on Urban Hydrological Response Sensitivity, *Water Resources Research*, 55(4), 3375-3390.
463 doi:10.1029/2018WR024143
464 Downer, C. W., and F. L. Ogden (2004), GSSHA: Model to simulate diverse stream flow producing processes, *Journal of*
465 *Hydrologic Engineering*, 9(3), 161-174. doi:10.1061/(ASCE)1084-0699(2004)9:3(161)
466 Downer, C. W., and F. L. Ogden (2006), Gridded Surface Subsurface Hydrologic Analysis (GSSHA) User's Manual;
467 Version 1.43 for Watershed Modeling System 6.1.
468 Emmanuel, I., H. Andrieu, E. Leblois, and B. Flahaut (2012), Temporal and spatial variability of rainfall at the urban
469 hydrological scale, *Journal of Hydrology*, 430-431, 162-172. doi:10.1016/j.jhydrol.2012.02.013
470 Emmanuel, I., H. Andrieu, E. Leblois, N. Janey, and O. Payrastre (2015), Influence of rainfall spatial variability on rainfall–
471 runoff modelling: Benefit of a simulation approach?, *Journal of Hydrology*, 531, 337-348.
472 doi:10.1016/j.jhydrol.2015.04.058
473 Faurès, J.-M., D. C. Goodrich, D. A. Woolhiser, and S. Sorooshian (1995), Impact of small-scale spatial rainfall variability
474 on runoff modeling, *Journal of Hydrology*, 173(1), 309-326. doi:10.1016/0022-1694(95)02704-S
475 Fulton, R. A., J. P. Breidenbach, D.-J. Seo, D. A. Miller, and T. O'Bannon (1998), The WSR-88D rainfall algorithm,
476 *Weather and Forecasting*, 13(2), 377-395. doi:10.1175/1520-0434(1998)013<0377:TWRA>2.0.CO;2
477 Galster, J. C., F. J. Pazzaglia, B. R. Hargreaves, D. P. Morris, S. C. Peters, and R. N. Weisman (2006), Effects of urbanization
478 on watershed hydrology: The scaling of discharge with drainage area, *Geology*, 34(9), 713-716. doi:10.1130/g22633.1
479 Gebremichael, M., and W. F. Krajewski (2004), Assessment of the statistical characterization of small-scale rainfall
480 variability from radar: Analysis of TRMM ground validation datasets, *Journal of Applied Meteorology*, 43(8), 1180-1199.
481 doi:10.1175/1520-0450(2004)043<1180:AOTSCO>2.0.CO;2
482 Gesch, D. B., M. J. Oimoen, S. K. Greenlee, C. A. Nelson, M. J. Steuck, and D. J. Tyler (2002), The national elevation data
483 set, *Photogrammetric Engineering and Remote Sensing*, 68(1), 5-11.
484 Gourley, J. J., et al. (2017), The FLASH Project: Improving the Tools for Flash Flood Monitoring and Prediction across
485 the United States, *Bulletin of the American Meteorological Society*, 98(2), 361-372. doi:10.1175/bams-d-15-00247.1
486 Krajewski, W., and J. Smith (2002), Radar hydrology: rainfall estimation, *Advances in water resources*, 25(8-12), 1387-
487 1394. doi:10.1016/S0309-1708(02)00062-3

Krajewski, W. F., A. Kruger, J. A. Smith, R. Lawrence, C. Gunyon, R. Goska, B.-C. Seo, P. Domaszczynski, M. L. Baeck, and M. K. Ramamurthy (2011), Towards better utilization of NEXRAD data in hydrology: an overview of Hydro-NEXRAD, *Journal of hydroinformatics*, 13(2), 255-266. doi:10.2166/hydro.2010.056

Lin, N., J. A. Smith, G. Villarini, T. P. Marchok, and M. L. Baeck (2010), Modeling extreme rainfall, winds, and surge from Hurricane Isabel (2003), *Weather and forecasting*, 25(5), 1342-1361. doi:10.1175/2010WAF2222349.1

Lindner, G. A., and A. J. Miller (2012), Numerical modeling of stage-discharge relationships in urban streams, *Journal of Hydrologic Engineering*, 17(4), 590-596.

Lu, P., J. A. Smith, and N. Lin (2017), Spatial Characterization of Flood Magnitudes over the Drainage Network of the Delaware River Basin, *Journal of Hydrometeorology*, 18(4), 957-976. doi:10.1175/jhm-d-16-0071.1

Maryland, S. o. (1982), Department of the Environment : Water management, stormwater management.

Meierdiercks, K. L., J. A. Smith, M. L. Baeck, and A. J. Miller (2010), Analyses of urban drainage network structure and its impact on hydrologic response, *JAWRA Journal of the American Water Resources Association*, 46(5), 932-943.

Moreau, E., J. Testud, and E. Le Bouar (2009), Rainfall spatial variability observed by X-band weather radar and its implication for the accuracy of rainfall estimates, *Advances in Water Resources*, 32(7), 1011-1019. doi:10.1016/j.advwatres.2008.11.007

Morin, E., D. C. Goodrich, R. A. Maddox, X. Gao, H. V. Gupta, and S. Sorooshian (2006), Spatial patterns in thunderstorm rainfall events and their coupling with watershed hydrological response, *Advances in Water Resources*, 29(6), 843-860.

Nash, J. E., and J. V. Sutcliffe (1970), River flow forecasting through conceptual models part I — A discussion of principles, *Journal of Hydrology*, 10(3), 282-290. https://doi.org/10.1016/0022-1694(70)90255-6

Nelson, P. A., J. A. Smith, and A. J. Miller (2006), Evolution of channel morphology and hydrologic response in an urbanizing drainage basin, *Earth Surface Processes and Landforms*, 31(9), 1063-1079. doi:10.1002/esp.1308

Nikolopoulos, E. I., M. Borga, D. Zoccatelli, and E. N. Anagnostou (2014), Catchment-scale storm velocity: Quantification, scale dependence and effect on flood response, *Hydrological Sciences Journal*, 59(7), 1363-1376. doi:10.1080/02626667.2014.923889

Ntelekos, A. A., J. A. Smith, M. L. Baeck, W. F. Krajewski, A. J. Miller, and R. Goska (2008), Extreme hydrometeorological events and the urban environment: Dissecting the 7 July 2004 thunderstorm over the Baltimore MD Metropolitan Region, *Water Resources Research*, 44(8), 1-19. doi:10.1029/2007WR006346

Ochoa-Rodriguez, S., L.-P. Wang, A. Gires, R. D. Pina, R. Reinoso-Rondinel, G. Bruni, A. Ichiba, S. Gaitan, E. Cristiano, and J. van Assel (2015), Impact of spatial and temporal resolution of rainfall inputs on urban hydrodynamic modelling outputs: A multi-catchment investigation, *Journal of Hydrology*, 531(2), 389-407. doi:10.1016/j.jhydrol.2015.05.035

Ogden, F. L., N. Raj Pradhan, C. W. Downer, and J. A. Zahner (2011), Relative importance of impervious area, drainage density, width function, and subsurface storm drainage on flood runoff from an urbanized catchment, *Water Resources Research*, 47(12). doi:10.1029/2011wr010550

Paschalis, A., S. Fatichi, P. Molnar, S. Rimkus, and P. Burlando (2014), On the effects of small scale space–time variability of rainfall on basin flood response, *Journal of Hydrology*, 514, 313-327. doi:10.1016/j.jhydrol.2014.04.014

Peleg, N., F. Blumensaat, P. Molnar, S. Fatichi, and P. Burlando (2017), Partitioning the impacts of spatial and climatological rainfall variability in urban drainage modeling, *Hydrology and Earth System Sciences*, 21(3), 1559. doi:10.5194/hess-21-1559-2017

Perez, G., R. Mantilla, W. F. Krajewski, and D. B. Wright (2019), Using Physically Based Synthetic Peak Flows to Assess Local and Regional Flood Frequency Analysis Methods, *Water Resources Research*, 55(11), 8384-8403. doi:10.1029/2019WR024827

Pickett, S. T. A., and M. L. Cadenasso (2006), Advancing urban ecological studies: Frameworks, concepts, and results from the Baltimore Ecosystem Study, *Austral Ecology*, 31(2), 114-125. doi:10.1111/j.1442-9993.2006.01586.x

Probst, P., M. N. Wright, and A. L. Boulesteix (2019), Hyperparameters and tuning strategies for random forest, *Wiley*

Interdisciplinary Reviews: Data Mining and Knowledge Discovery, 9(3), e1301. doi:10.1002/widm.1301
Rafieeinasab, A., A. Norouzi, S. Kim, H. Habibi, B. Nazari, D.-J. Seo, H. Lee, B. Cosgrove, and Z. Cui (2015), Toward high-resolution flash flood prediction in large urban areas – Analysis of sensitivity to spatiotemporal resolution of rainfall input and hydrologic modeling, *Journal of Hydrology*, 531, 370-388. doi:10.1016/j.jhydrol.2015.08.045
Rahman, A., P. E. Weinmann, T. M. T. Hoang, and E. M. Laurenson (2002), Monte Carlo simulation of flood frequency curves from rainfall, *Journal of Hydrology*, 256(3), 196-210. doi:10.1016/S0022-1694(01)00533-9
Saghafian, B., P. Y. Julien, and F. L. Ogden (1995), Similarity in catchment response: 1. Stationary rainstorms, *Water Resources Research*, 31(6), 1533-1541. doi:10.1029/95WR00518
Schellart, A. N. A., W. J. Shepherd, and A. J. Saul (2012), Influence of rainfall estimation error and spatial variability on sewer flow prediction at a small urban scale, *Advances in Water Resources*, 45, 65-75. doi:10.1016/j.advwatres.2011.10.012
Seo, B.-C., W. F. Krajewski, A. Kruger, P. Domaszczynski, J. A. Smith, and M. Steiner (2011), Radar-rainfall estimation algorithms of Hydro-NEXRAD, *Journal of Hydroinformatics*, 13(2), 277-291. doi:10.2166/hydro.2010.003
Sharif, H. O., A. A. Hassan, S. Bin-Shafique, H. Xie, and J. Zeitler (2010), Hydrologic modeling of an extreme flood in the Guadalupe River in Texas, *JAWRA Journal of the American Water Resources Association*, 46(5), 881-891. doi:10.1111/j.1752-1688.2010.00459.x
Sharif, H. O., S. Chintalapudi, A. A. Hassan, H. Xie, and J. Zeitler (2013), Physically Based Hydrological Modeling of the 2002 Floods in San Antonio, Texas, *Journal of Hydrologic Engineering*, 18(2), 228-236. doi:10.1061/(ASCE)HE.1943-5584.0000475
Smith, B., J. Smith, M. Baeck, and A. Miller (2015), Exploring storage and runoff generation processes for urban flooding through a physically based watershed model, *Water Resources Research*, 51(3), 1552-1569. doi:10.1002/2014WR016085
Smith, B. K., J. A. Smith, M. L. Baeck, G. Villarini, and D. B. Wright (2013), Spectrum of storm event hydrologic response in urban watersheds, *Water Resources Research*, 49(5), 2649-2663. doi:10.1002/wrcr.20223
Smith, J. A., and W. F. Krajewski (1991), Estimation of the mean field bias of radar rainfall estimates, *Journal of Applied Meteorology*, 30(4), 397-412.
Smith, J. A., M. L. Baeck, K. L. Meierdiercks, A. J. Miller, and W. F. Krajewski (2007), Radar rainfall estimation for flash flood forecasting in small urban watersheds, *Advances in Water Resources*, 30(10), 2087-2097. doi:10.1016/j.advwatres.2006.09.007
Smith, J. A., M. L. Baeck, J. E. Morrison, P. Sturdevant-Rees, D. F. Turner-Gillespie, and P. D. Bates (2002), The regional hydrology of extreme floods in an urbanizing drainage basin, *Journal of Hydrometeorology*, 3(3), 267-282. doi:10.1175/1525-7541(2002)003<0267:TRHOEF>2.0.CO;2
Smith, J. A., A. J. Miller, M. L. Baeck, P. A. Nelson, G. T. Fisher, and K. L. Meierdiercks (2005a), Extraordinary Flood Response of a Small Urban Watershed to Short-Duration Convective Rainfall, *Journal of Hydrometeorology*, 6(5), 599-617. doi:10.1175/JHM426.1
Smith, J. A., M. L. Baeck, K. L. Meierdiercks, P. A. Nelson, A. J. Miller, and E. J. Holland (2005b), Field studies of the storm event hydrologic response in an urbanizing watershed, *Water Resources Research*, 41(10), W10413(10415). doi:10.1029/2004wr003712
Smith, J. A., M. L. Baeck, G. Villarini, C. Welty, A. J. Miller, and W. F. Krajewski (2012), Analyses of a long-term, high-resolution radar rainfall data set for the Baltimore metropolitan region, *Water Resources Research*, 48(4), 1-14. doi:10.1029/2011wr010641
ten Veldhuis, M. C., Z. Zhou, L. Yang, S. Liu, and J. Smith (2018), The role of storm scale, position and movement in controlling urban flood response, *Hydrology and Earth System Sciences*, 22(1), 417-436. 10.5194/hess-22-417-2018
Wright, D. B., J. A. Smith, and M. L. Baeck (2014a), Flood frequency analysis using radar rainfall fields and stochastic storm transposition, *Water Resources Research*, 50(2), 1592-1615. doi:10.1002/2013WR014224
Wright, D. B., R. Mantilla, and C. D. Peters-Lidard (2017), A remote sensing-based tool for assessing rainfall-driven

576 hazards, *Environmental Modelling & Software*, 90, 34-54. doi:10.1016/j.envsoft.2016.12.006
577 Wright, D. B., G. Yu, and J. F. England (2020), Six decades of rainfall and flood frequency analysis using stochastic storm
578 transposition: Review, progress, and prospects, *Journal of Hydrology*, 585, 124816. doi:10.1016/j.jhydrol.2020.124816
579 Wright, D. B., J. A. Smith, G. Villarini, and M. L. Baeck (2012), Hydroclimatology of flash flooding in Atlanta, *Water*
580 *Resources Research*, 48(4). https://doi.org/10.1029/2011wr011371
581 Wright, D. B., J. A. Smith, G. Villarini, and M. L. Baeck (2013), Estimating the frequency of extreme rainfall using weather
582 radar and stochastic storm transposition, *Journal of Hydrology*, 488, 150-165. doi:10.1016/j.jhydrol.2013.03.003
583 Wright, D. B., J. A. Smith, G. Villarini, and M. L. Baeck (2014b), Long-term high-resolution radar rainfall fields for urban
584 hydrology, *Journal of the American Water Resources Association*, 50(3), 713-734. doi:10.1111/jawr.12139
585 Yang, L., J. A. Smith, M. L. Baeck, and Y. Zhang (2016), Flash flooding in small urban watersheds: Storm event hydrologic
586 response, *Water Resources Research*, doi:doi:10.1002/2015WR018326. doi:10.1002/2015WR018326
587 Yang, Y., L. Sun, R. Li, J. Yin, and D. Yu (2020), Linking a Storm Water Management Model to a Novel Two-Dimensional
588 Model for Urban Pluvial Flood Modeling, *International Journal of Disaster Risk Science*, 11(4), 508-518. 10.1007/s13753-
589 020-00278-7
590 Yin, J., D. Yu, Z. Yin, M. Liu, and Q. He (2016), Evaluating the impact and risk of pluvial flash flood on intra-urban road
591 network: A case study in the city center of Shanghai, China, *Journal of Hydrology*, 537, 138-145.
592 https://doi.org/10.1016/j.jhydrol.2016.03.037
593 Yu, G., D. B. Wright, Z. Zhu, C. Smith, and K. D. Holman (2019), Process-based flood frequency analysis in an agricultural
594 watershed exhibiting nonstationary flood seasonality, *Hydrol. Earth Syst. Sci.*, 23(5), 2225-2243. doi:10.5194/hess-23-
595 2225-2019
596 Zhou, Z., J. A. Smith, D. B. Wright, M. L. Baeck, and S. Liu (2019), Storm catalog-based analysis of rainfall heterogeneity
597 and frequency in a complex terrain, *Water Resources Research*, 55(3), 1871-1889. doi:10.1029/2018WR023567
598 Zhou, Z., J. A. Smith, L. Yang, M. L. Baeck, M. Chaney, M.-C. Ten Veldhuis, H. Deng, and S. Liu (2017), The complexities
599 of urban flood response: Flood frequency analyses for the Charlotte Metropolitan Region, *Water Resources Research*, 53(8),
600 7401-7425. doi:10.1002/2016WR019997
601 Zhu, Z., D. B. Wright, and G. Yu (2018), The Impact of Rainfall Space-Time Structure in Flood Frequency Analysis, *Water*
602 *Resources Research*, 54(11), 8983-8998. doi:10.1029/2018wr023550
603 Zoccatelli, D., M. Borga, A. Viglione, G. B. Chirico, and G. Blöschl (2011), Spatial moments of catchment rainfall: rainfall
604 spatial organisation, basin morphology, and flood response, *Hydrology and Earth System Sciences*, 15(12), 3767-3783.
605 10.5194/hess-15-3767-2011
606
607
608
609

Appendix A

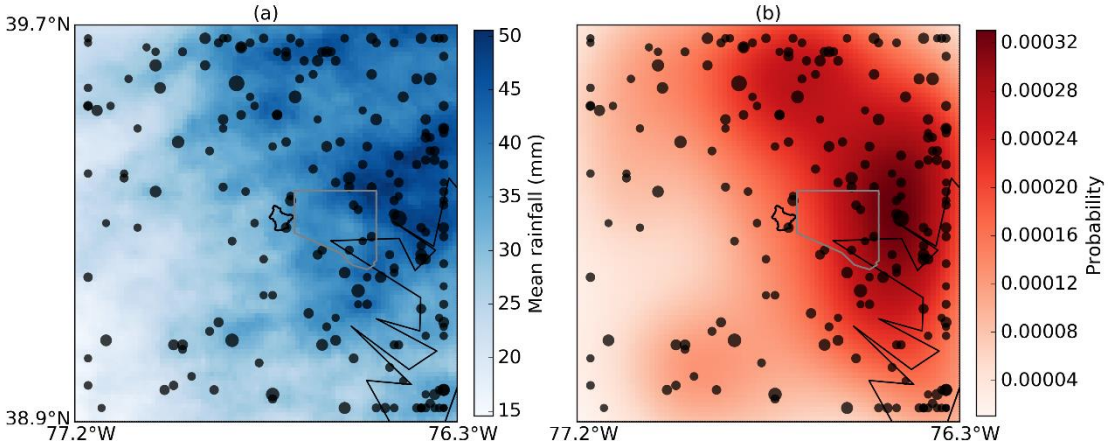

Figure A1: Maps of mean storm total rainfall (a) and probability of storm occurrence (b) for the 200 storms in the 3-h storm catalog (The black dot indicates the location of rainfall centroid).

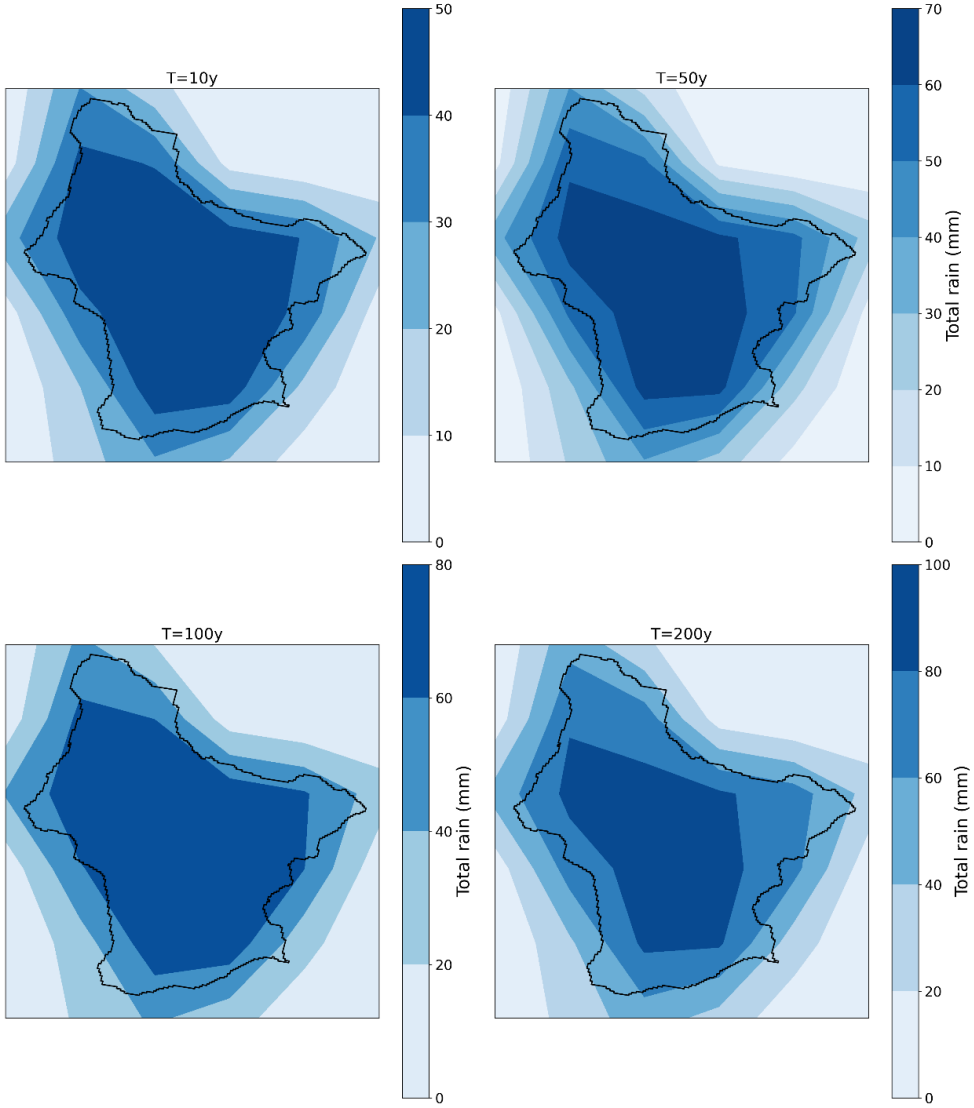

Figure A2: Composite map of rainfall distribution for the 10-y, 50-y, 100-y and 200-y return periods.

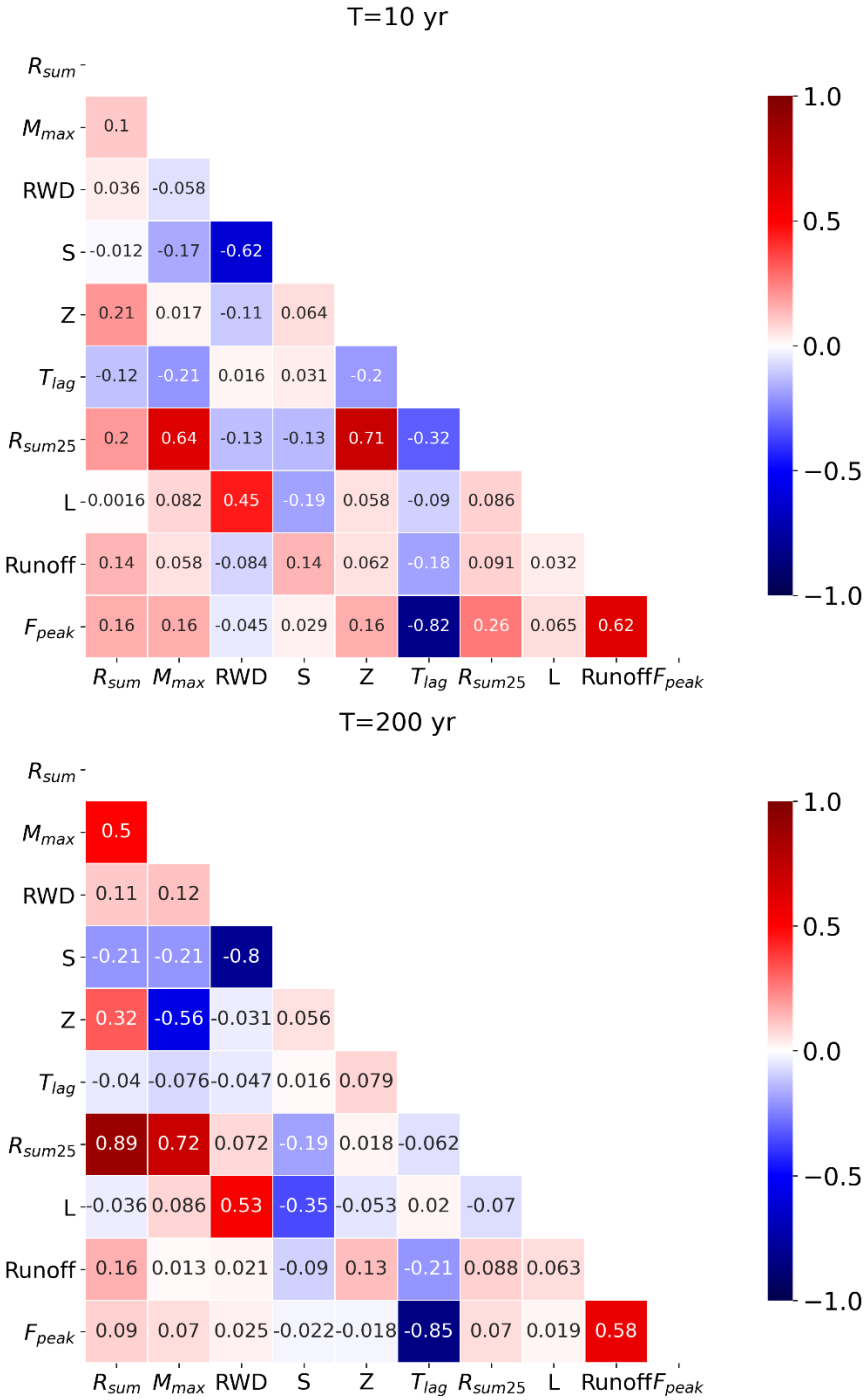

Figure A3: Correlation between space-time rainfall structure and flood responses at Franklintown under 10-yr and 200-yr return periods.

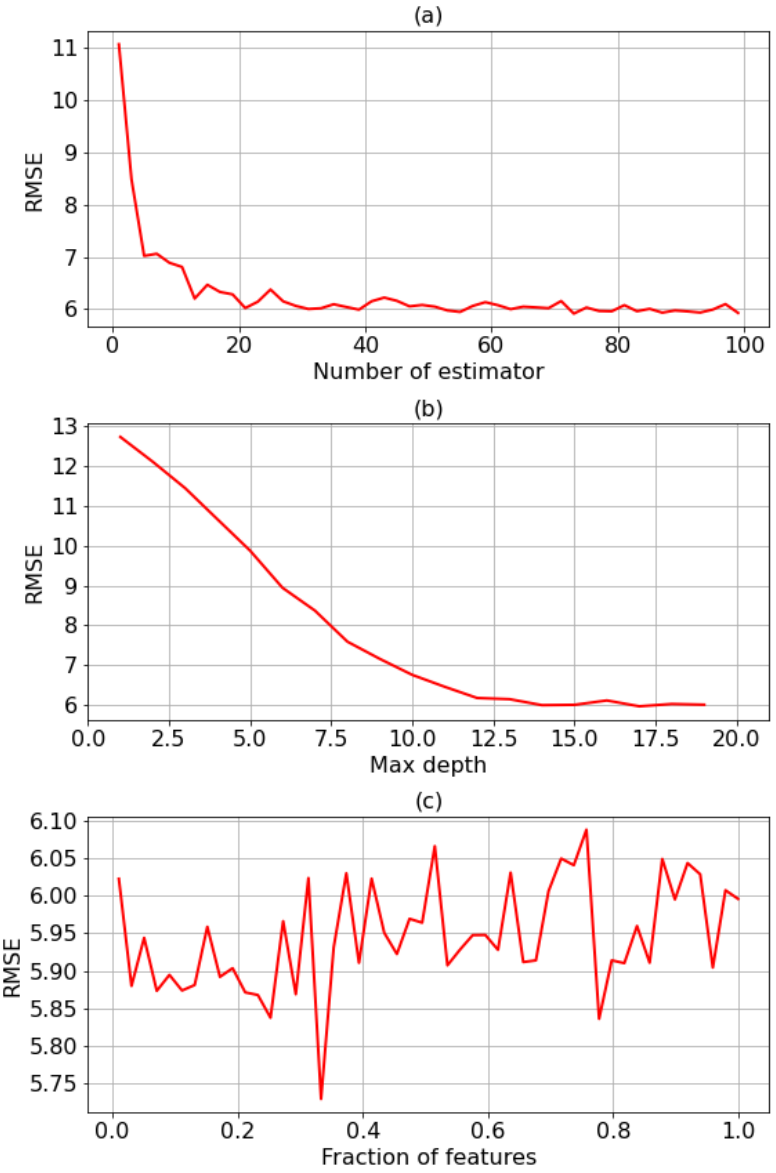

Figure A4: The parameter tuning process of RF model (use RMSE for example)